Photogrammetrie • Fernerkundung • Geoinformation 3/2007, S. 207–214, 5 figs.

Simultaneous 3D-Flow Field and Compliant Wall Measurements in an Abdominal Aortic Aneurysm Flow using Scanning-PTV

Klaus Werner Hoyer*, Joseph Knight, Markus Holzner, Michele Guala & Wolfgang Kinzelbach, Zürich

Keywords: Medicine, tomographic scanning, index matching, scanning particle tracking velocimetry, flow phantom

Abstract: We combine well established particle tracking with wall surface measurements using tomographic scanning and present results for the non-stationary 4D – flow field within an abdominal aortic aneurysm (AAA) phantom. It was manufactured from an optically homogeneous but slightly opaque silicone having an index of refraction $n = 1.414$. The fluid used is a mixture of water and glycerol to match the index of refraction of the silicone to render the region of interest undistorted. The 3D data is acquired in two ways. First full volume illumination and spectral separation of Rhodamine labelled particles is used to obtain the flow field. In a second experiment, a scanning light sheet illumination for the detection of the aorta wall is used. Both experiments are phase locked to the pulsating beat of the pump. We use a set of four high speed cameras, which were calibrated using a standard PIV calibration target placed parallel at two separate planes within the region of interest. In addition to the seeded particles, which we identify and track in time, the aneurism wall lights up across the cut with the laser plane and we will now also extract the surface of the moving interior wall through proper epipolar constraints, e. g. their intersection with a filtered edge detection map.

Previous measurements and attempts of different groups (MRI, DNS) to unify the stationary flow field data have shown the necessity to obtain the compliant wall motion simultaneously with the flow field boundary conditions. This paper addresses this issue to meet all necessary requirements that will allow further development of a numerical simulation tool.

* Corresponding author.

Kurzfassung: *Simultane Messung eines pulsierenden Geschwindigkeitsfeldes und der bewegten Gefäßwand eines abdominalen Aortenaneurysmas mit Scanning PTV.* Wir kombinieren Particle Tracking Velocimetry und tomographisches Laser Sheet Scanning, um das Geschwindigkeitsfeld und die Wandbewegung eines abdominalen Aortenaneurysmas (AAA) während pulsierendem Durchfluss zu bestimmen. Das AAA-Phantom besteht aus optisch homogenem, flexiblem Silikon mit Brechungsindex $n = 1.414$ und leicht milchiger Färbung. Als Testflüssigkeit wurde eine Mixtur aus Wasser und Glycerin mit gleichem Brechungsindex gemischt, um das Beobachtungsvolumen verzerrungsfrei abbilden zu können. Die 3D Daten werden auf zwei Methoden erzielt. Zuerst wird das gesamte Beobachtungsvolumen beleuchtet und die Emission der beigefügten Flüssigkeitsmarker (Rhodamine Partikel) durch einen Gelbfilter vom Hintergrund getrennt. In einem folgenden Experiment wird die Aorta-Wand mit einer dünnen, senkrecht zu ihrer Ebene bewegten, Lichtschicht durchstrahlt. Dasselbe Kamerasystem, jedoch ohne Gelbfilter, erlaubt nun die Wandkoordinaten aus den im Laserschnitt beleuchteten Querschnitten im Raum zu rekonstruieren. Beide Experimente sind über eine im Bild platzierte LED mit dem Puls der Pumpe synchronisiert und erlauben so, ein phasengemitteltes Geschwindigkeitsfeld und die zugehörige Wandbewegung als Funktion der Zeit darzustellen.

Frühere Versuche verschiedener Gruppen (MRI, DNS) zeigten, dass beide Informationen im gleichen Experiment zu messen sind, um ein geschlossenes System inklusive der zeitlich abhängigen Randbedingungen zu erhalten. Dieses dient dann als Testfall für die Weiterentwicklung der numerischen Methoden für den allgemeinen Fall.

1432-8364/07/2007/0207 $ 2.25

1 Introduction

1.1 *Motivation*

The quantitative analysis and modelling of fluid flow in humans has become an increasingly important tool for decision making regarding the course of action for treatment. In patients with an aortic aneurysm, the risks of surgery have to be weighted against the risks of rupture. To date, the main decision criterion for or against surgical intervention is a critical aneurysm diameter of $D = 5\,\text{cm}$.

Whereas this criterion is an empirically found result that should save most peoples' lives, each aneurism exhibits its own flow topology. Additional fluid stresses on the arterial walls stem from flow redirection, flow separation and possibly wall attached vortex cores. Generally these additional stresses generate within the aneurism due to the sudden increase diameter and therefore act primarily on the arterial wall cells that have already weakened considerably. The local nature of these repetitive alternating fluid flow stresses may contribute significantly to ones individual risk, especially when the wall has lost enough elasticity and support tissue to actually collapse locally during the low pressure phase.

The final goal of this cooperative effort is to have a reliable numerical simulation tool that incorporates the moving geometry and time dependent fluxes from individual patient MRI data to help in the decision process.

1.2 *Aims*

We aim to provide a complete experimental data set that allows the necessary verification and optimization of a numerical flow simulation, given the fluctuating wall surface and flux or pressure boundary conditions at the inlet and exits. Although the phantom geometry is modelled after an individual patient, the experimental setup will not simulate the exact flow in the patient mainly due to differences in the outlet impedances and the differences in the structural support. Nevertheless it will provide a viable data set, being a regular solution of the Navier-Stokes equations under the given boundary conditions.

Previous work using index matched liquids for optical flow measurements in complex geometries were pioneered by Edwards & Dybbs 1984 (LDA in rod bundles) and later expanded by Hopkins et al. 2000 (PIV in a nasal cavity). Here additionally we allow compliant wall motion compared to the previous investigations.

2 Material and Methods

2.1 *Index matching*

The AAA wall material is a permanently cured but flexible silicone from DOW Chemicals and was manufactured by repeatedly brushing the surface of a $\lambda = 3/2$ scaled up wax positive and curing the layer to the elastic state from the initially viscous liquid state. During the liquid state of the curing process, the positive wax geometry has to be constantly tumbled around in a specially designed rotating fixture to avoid large irregularities in the wall thickness.

The material exhibits a homogeneous index of refraction that has been matched using an approximate (40 : 60) mixture of glycerol and water. During the mixing and matching, the refractive index of the solution was repeatedly measured using a Bellingham + Stanley Eclipse 45–41 refractometer, which allowed approaching the ideal mixture asymptotically.

2.2 *Full volume illumination for particles phase*

As tracer particles we added Rhodamine labelled particles with a nominal size distribution of $64\,\mu\text{m} < d_{90} < 128\,\mu\text{m}$. It was necessary to use labelled particles to increase the signal to noise ratio. Unfortunately, the silicone material was more opaque than it should ideally have been. Although certain opaqueness is desirable, too much scatter from the wall increases the background grey value and also blocks light especially to re-

gions where it has to pass multiple wall segments. The particle phase was therefore measured separately from the wall acquisition described further below.

To measure the particle phase, we used an expanded Ar-Ion laser beam and yellow filters on the cameras to block the scattered light (488 and 514 nm wavelength), from the aneurism wall. A separate camera calibration was obtained for the setup with filters since it was necessary to touch the cameras to mount the mirrors. The camera exposure was over the entire frame at a camera frame rate of $f_C = 250$ Hz.

2.3 *Scanning laser sheet illumination for wall*

Our laser sheet is obtained by expanding an Ar-Ion laser beam of approximately 2.5 mm diameter using a cylindrical lens. The sheet thickness at the observation volume adjusts to approximately $d_{LS} = 1$ mm using a long focal length cylindrical lens. The laser beam reflects from rotating 16-face cylindrical mirror and a passes through a spherical lens to parallelize the beam. The prism was closed loop controlled using National Instruments motion control hardware. The horizontally scanning beam now expands to a sheet using a $f = 8.5$ mm focal length cylindrical lens having a maximum length $l = 80$ mm. The scanning laser sheet then is mirrored directly to the region of interest such that the light passes through the model in the least self obstructing way, possibly compromising the ideal case of the scan direction being as aligned to the camera axis as possible to maximize data yield. The wall data was acquired having the prism rotating at $f_{VS} = 11$ Hz. Camera frame rate was set at $f_C = 500$ Hz and shutter set to 1 ms to obtain stop action images.

2.4 *Camera setup and image splitter*

We use a set of four highspeed cameras (Microtron with resolution 1280 k by 1024 k @ 12 µm square pixels) with C-mount $f = 25$ mm focal length lenses set with two 5 mm spacers and at f#16 to maximize depth of field. Additionally a yellow filter reduced the direct scatter of the laser light and passed the Rhodamine emitted light essentially unhindered. This allowed additional signal improvement for the fluid phase tracking. The cameras are set to view a common region of interest.

3 Data acquisition and processing

3.1 *Camera calibration*

The camera calibration is achieved using a standard PIV target positioned at two known planes separated approximately as to border the front and back of the region of interest with respect to the camera axis. The back calibration image was taken through the AAA phantom. This image was high pass filtered, after which edge artefacts from the phantom were removed, whereas the front calibration was imaged directly. To give an impression for the index match quality we show the original back calibration image in Fig. 1.

Together with a target file of the "true" 3D coordinates, this image file allows determination of the inner and outer camera parameters with respect to a chosen coordinate system. The calibration, the particle recognition and the stereoscopic matching through the multimedia geometry is detailed

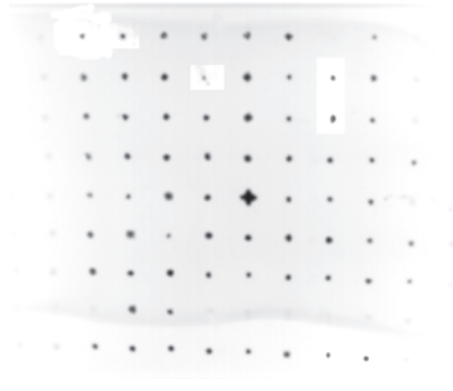

Fig. 1: Processed back plane calibration image as seen by one camera. In the second from bottom row one recognizes the slightly opaque AAA phantom wall (particles were removed).

in Maas (1992). The calibration of the camera model allowed identification and stereo-matching of about 400 particles per slice. The positioning accuracy is about 50 µm in the normal to and about 300 µm parallel to the camera axis. The decreased resolution along the optical axis can be explained with the large working distance when imaging a relatively large region of interest using the 4 way splitter geometry and a 25 mm focal length lens. A shorter focal length lens may also help to improve this compromise.

3.2 *Camera trigger*

The camera is being triggered in ''random reset''-mode which allows triggering to the rotating prism or each new start of the laser scan. On the trigger, the camera timer is reset after which a set number of images are taken at a pre-programmed frame rate. In our case we obtained 20 images at 500 Hz camera frame rate per trigger.

3.3 *Image sequence*

In SPTV we use a laser sheet that scans perpendicular to its plane, whereas a camera repeatedly takes a rapid image sequence. To illustrate the process, we have added a filmstrip image of a volume scan through the region of interest

As a result of the fast sequential image acquisition we have an observation volume that is gathered with increasing time stamp, e. g. the far planes are scanned after the near planes. For the tracking and post-processing it is desirable to have all data interpolated to a single time stamp for each volume scan. The detailed code adaptations for

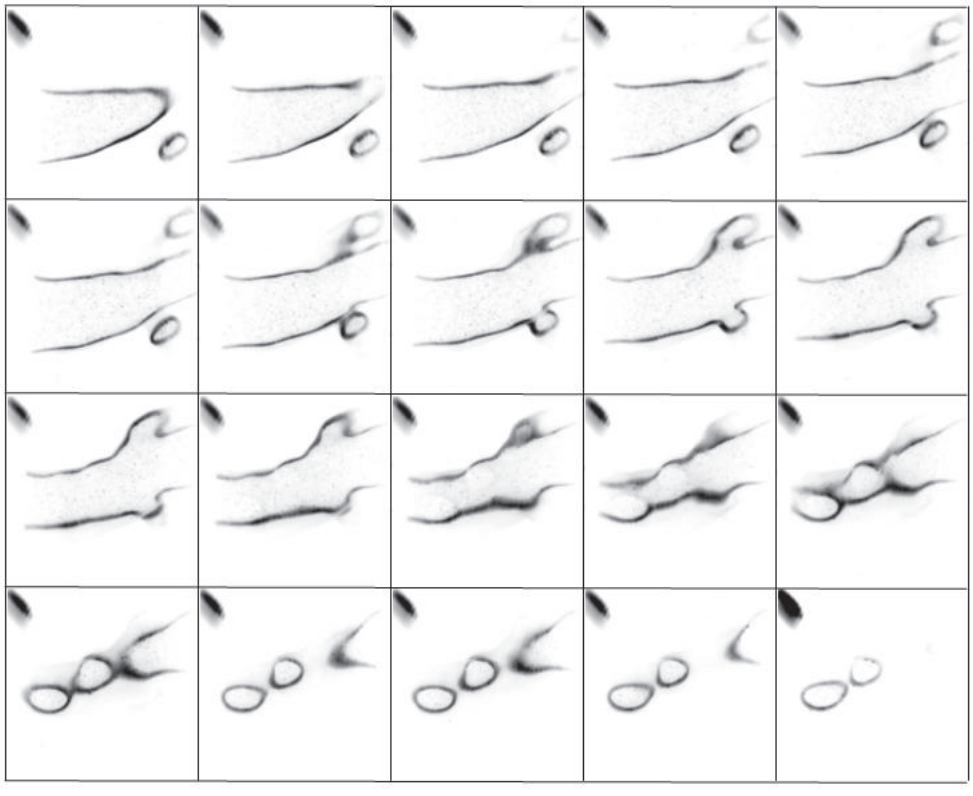

Fig. 2: Filmstrip of one volume scan through the aorta as imaged by one camera view. Time progresses from left to right and from top to bottom. The camera frame rate from this earlier is 2 kHz and is acquired within 1/100 s.

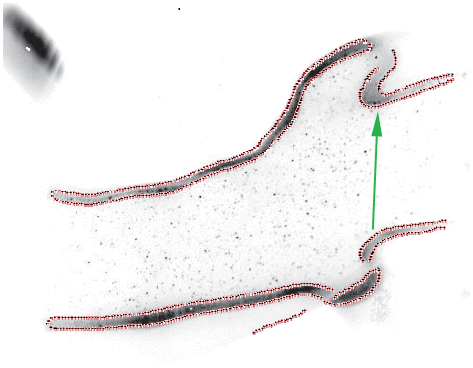

Fig. 3: Top/left quarter of the imager chip with typical raw data (grey) and pearl-string contour (red). The green arrow is parallel to the laser light. Both the illumination and the observation paths are partly obscured by wall material; especially noticeable as dark region (top right) and as edge artefact through the lower segment (bottom right), respectively.

SPTV post-processing have been published recently Hoyer et al. (2005). We tracked the particle data sequence using a correlation based approach detailed in Hoyer et al. (2006). For now, we will focus on the edge detection algorithm used to determine the wall coordinates. Fig. 3 shows a single slice of raw data of the top/left 512^2 pixels, where seed particles and aortic wall are visible being illuminated by a thin slice. The edge detected by the image pre-processing is also highlighted as red pointed line. We can see that the obstruction of the illuminated region by dark wall material leads to false edges, visible in edge detected the lower right artery. Since these false edges do not generally result in matched edges, they do not show up in the result. Only edges that have stereoscopic matches are determined real, data that does not result in stereoscopic matches is discarded.

The scanning laser sheet adds an additional dynamic thickness to the width of the laser sheet. When scanning the sheet perpendicular to its plane, the illuminated region grows linearly with time. To obtain a sharp contour it is therefore desirable to have a thin static sheet and a short exposure time. Since the particle recognition requires the shutter to be open for the inverse of the frame rate, we can only increase the frame rate to minimize this dynamic effect. For the

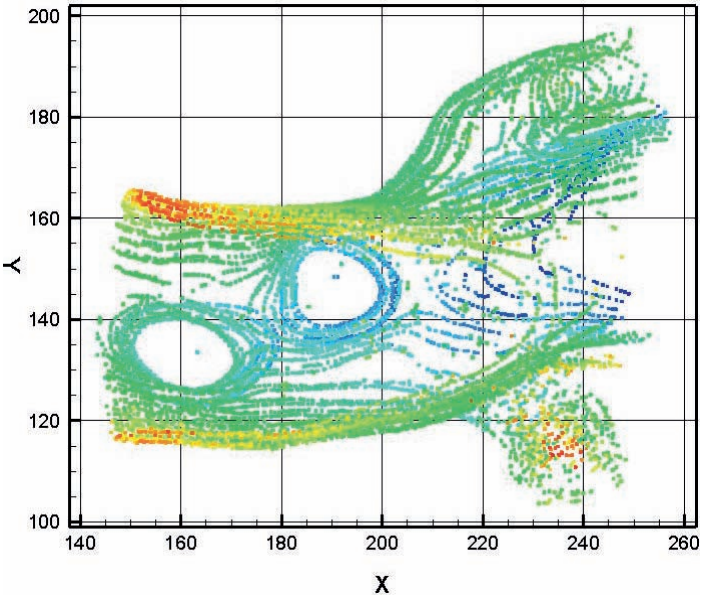

Fig. 4: Inner and outer surface contours of the aortic wall compiled from 20 slices. Colours indicates Z-coordinate (red near/blue far) (units in [mm]).

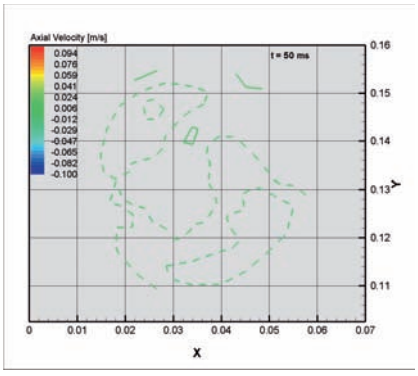

a

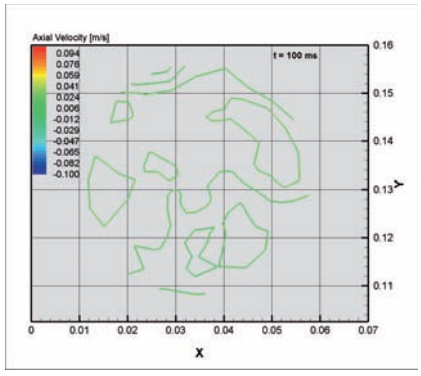

b

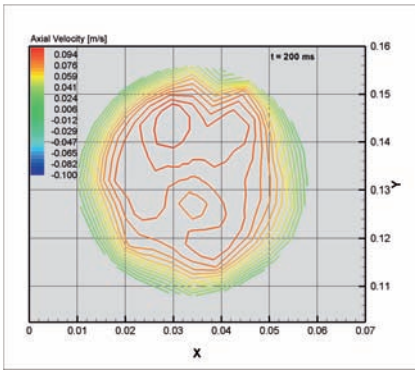

c

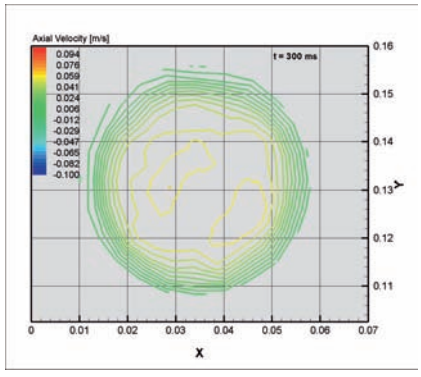

d

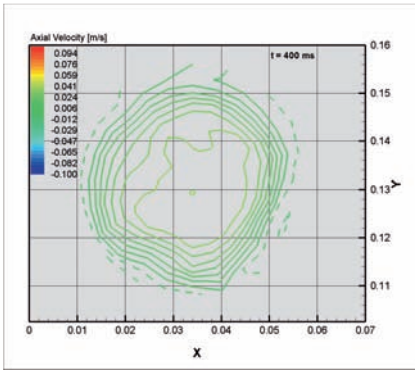

e

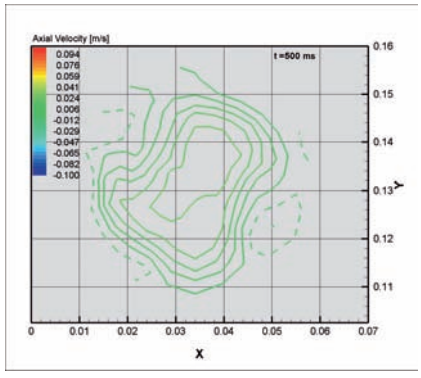

f

Fig. 5a–f: Axial Velocity profile over the artery cross section at different instances in time. Dashes lines resemble negative velocities. Data is interpolated using 16 phase locked pulses overall.

surface extraction, the images were pre-processed to remove the particles and to increase the signal from the wall scatter using low pass filtering and gamma correction. The edge detection and segmentation was achieved using the LabView image processing toolbox.

3.4 *Surface extraction*

The surface extraction is achieved by processing the edge segments as strings of particles. Therefore we generated finely discretized lines of "particles" along all edge sequences to feed to the particle recognition and matching code. When the line is discretized in increments smaller than the tolerance to the epipolar line, the stereoscopic matching algorithm will find some candidates and chooses the match with the least error in every image as long as a common edge has been detected. The additional noise introduced to the wall coordinate is directly related to the discretization and thus can be reduced to levels comparable with regular particle recognition uncertainties. For the current application, memory or processing time restraints have not surfaced using this approach.

Fig. 4 shows the reconstructed volume obtained with the described edge detection displaying the main abdominal aortic branches supplying kidneys and digestive tract. The branch leading out to the bottom right exhibits decreased resolution and possibly artefacts due to the mentioned obstruction in the observation path. This obstruction can be reduced by processing also unambiguous stereo pairs. This is possible only when the location of the arbitrarily inclined scanning plane is modelled correctly in time, so that the epipolar lines can be kept as short as possible. This can be done in a second step after processing the images in a first step using little restriction on the length of the epipolar lines. The arbitrary inclination and scanning direction is necessary to avoid obstruction of the illumination path. This iterative second step is not yet implemented and the particle cloud presented in Fig. 4 was compiled from triplets and quadruplets, e. g. common points recognized in three and four cameras simultaneously, respectively. Possibly also other topological features such as the grey value gradient will be needed to sort out doublet match ambiguities from opposite surfaces.

3.5 *Flow field extraction*

The pulsating flow field in the observed experiment (see Fig. 5a–f) has a large variation from almost zero velocity to a maximum of $U = 0.15\,\mathrm{m/s}$ which leads to a Reynolds number of $\mathrm{Re} = 450$ based on the aorta diameter $D = 0.03\,\mathrm{m}$ and kinematic viscosity of the water glycerol mixture $\nu = 10^{-5}\,\mathrm{m^2/s}$.

Particle tracking was achieved using the four time frame tracking algorithm described previously. We were also using a yellow filter to increase the signal to noise ratio for the particles, however had trouble recognizing particles in the darker regions, which is especially true at the Gaussian tails of the laser sheet intensity. Contrary to the image preprocessing for the wall surface, the particle images were high pass filtered.

4 Conclusion

We are presenting a highly resolved flow field within a replica of an abdominal aortic aneurysm using SPTV for the illumination of the tracer particles and the phantom wall. From a total of 11500 detected particles per volume scan, 4000 interpolated trajectories remained after tracking and trajectory interpolation. The scattered light from the opaqueness of the phantom wall material exceeds by far the signal from the particle images. Therefore we used spectral separation between the excitation at 514 nm and the particle Rhodamine emission using a yellow filter. The model wall was more opaque than necessary which resulted in reduced data quality and necessitated workarounds. The particle recognition and matching algorithm allows essentially an arbitrary orientation of the illuminating light sheet, which is necessary to optimize the light path through the model phantom with

respect to the obstruction of the incoming light. Although optimally perpendicular to the common camera symmetry line, the direction and motion ot the scanning sheet has to avoid also connection tubing and fittings within the model tank. The optical access of both illumination and observation has to be carefully judged designing and building a generally customized glass-walled container. We present a single observation volume of only a part of the entire flow phantom. We plan to repeat and optimize the measurements over the entire phantom to obtain a dynamic flow field and wall motion map as an experimental baseline and boundary conditions to allow improvement of the direct numerical simulation of such flow problems.

Acknowledgements

We wish to express our gratitude to the Swiss national science foundations CO-ME program sponsored through the National Centres of Competence in Research (NCCR).

References

Edwards, R.V. & Dybbs, A., 1984: Refractive index matching for velocity measurements in complex geometries. – TSI Quarterly, Volume X, Issue 4.

Hopkins, L.M., Kelly, J.T., Wexler, A.S. & Prasad. A.K., 2000: Particle image velocimetry in complex geometries. – Experiments in Fluids, 29: 91–95.

Hoyer, K., Holzner, M., Lüthi, B., Guala, M., Liberzon, A. & Kinzelbach, W., 2005: 3D Scanning particle tracking velocimetry. – Experiments in Fluids, 39: 923–934.

Hoyer, K., Holzner, M. & Kinzelbach, W., 2006: Correlation based particle tracking Velocimetry. – 5th International Symposium on Turbulence, Heat and Mass Transfer, Dubrovnik, Croatia, September 25–29, 2006.

Maas, H.-G., 1992: Doctoral thesis: Digitale Photogrammetrie in der dreidimensionalen Strömungsmesstechnik. – Dissertation ETH Nr.: 9665.

Address of the authors:

Dr. sc. tech. Klaus Werner Hoyer,
Tel. +41-44-6333068, Fax: +41-44-6331061

M.Sc. Biomed.Engineering Joseph Knight
Dipl.-Ing. Markus Holzner
Dr. Envir. Engineering Michele Guala
Prof. Dr.-Ing. Wolfgang Kinzelbach

e-mail: (hoyer,holzner,guala,kinzelbach)@ifu.bau.ethz.ch,
joseph.knight@ltnt.iet.mavt.ethz.ch
ETH Zürich, CH-8093 Zürich, HIL G 37.1
Institut für Umweltingenieurwissenschaften (IfU), Professur für Grundwasser und Hydromechanik (GWH)

Manuskript eingereicht: Januar 2007
Angenommen: Januar 2007